International Journal of Multiphase Flow 132 (2020) 103397

Contents lists available at ScienceDirect

International Journal of Multiphase Flow

journal homepage: www.elsevier.com/locate/ijmulflow

Towards a model of bubble breakup in turbulence through experimental constraints☆

Yinghe Qi, Ashik Ullah Mohammad Masuk, Rui Ni*

Department of Mechanical Engineering, Johns Hopkins University, Baltimore, MD-21218, USA

ARTICLE INFO

Article history:
Received 8 May 2020
Revised 5 June 2020
Accepted 15 June 2020
Available online 18 July 2020

Keywords:
Bubble breakup
Turbulence
Breakup model
3D shape reconstruction

ABSTRACT

Complex bubble breakup in turbulence has been studied and modeled extensively by employing the population balance equation. This equation hinges on two quantities, i.e. daughter bubble size distribution and breakup frequency. Since there is no first-principle equation that can be solved to calculate these two quantities, many phenomenological models based on different physical mechanisms have been proposed. A large number of possible mechanisms at play leads to models with drastically different, and even contradictory, predictions. In contrast, experimental measurements of these two quantities, including several previous works and our own results collected in a vertical water tunnel that features a large homogeneous and isotropic region, seem to be consistent with one another. To resolve the difference between models and experiments, rather than following another physical argument, we approach the problem from a different direction by asking how to constrain a model based on experimental results. The specific constraints extracted from eight experimental results include: (i) direct measurements of daughter bubble size distribution; (ii) Super-Hinze-scale bubble size spectrum for constraining breakup frequency; (iii) Sub-Hinze-scale bubble size spectrum for modeling daughter bubble size distribution; (iv) Convergence time to an equilibrium state. Finally, based on these experimental constraints, a new breakup model that incorporates a corrected formulation for breakup frequency as well as a simplified function for daughter bubble distribution is developed to meet all constraints. Although the new model is deliberately not connected to any specific physical arguments for simplification, it appears to be robust and consistent with all experimental constraints mentioned.

1. Introduction

Bubble fragmentation in turbulence eventually determines bubble size spectrum and the interfacial area concentration (Kocamustafaogullari and Ishii, 1995), which are crucial to many multiphase flow applications that involve complex interfacial heat and mass transfer. This process is often modelled using the population balance equation (for details, see Section 2), which is a Boltzmann-type equation. Within this equation, there are two important parameters, one of which is daughter bubble size distribution. As its name suggests, it represents the size distribution of all daughter bubbles generated from breakup events. Since there is no first-principle method that can derive the daughter bubble size distribution, many models have been proposed, including statistical and phenomenological models. The statistical models assume that the size of daughter bubbles is a random variable following some simple distributions, including normal (Valentas et al., 1966; Coulaloglou and Tavlarides, 1977), Beta (Hsia and Tavlarides, 1983), and uniform distribution (Narsimhan et al., 1979; Prince and Blanch, 1990). More recently, the phenomenological models (Tsouris and Tavlarides, 1994; Luo and Svendsen, 1996; Martínez-Bazán et al., 1999b; Lehr et al., 2002; Hagesaether et al., 2002; Wang et al., 2003; Zhao and Ge, 2007; Han et al., 2011) start to gain popularity because they are usually formulated based on the process of bubble-eddy collision, which is more physical compared with the statistical methods. However, as we will discuss in Section 4.1, many of these phenomenological models result in drastically different daughter bubble size distributions that seem to be inconsistent with experimental findings.

For experiments, bubble breakup has been studied in many different flow configurations. Daughter bubble size distribution was directly measured in turbulent pipe flows by Hesketh et al. (1991) and turbulent jets by Rodríguez-Rodríguez et al. (2003) and Vejražka et al. (2018). In addition

☆ We acknowledge the financial support from the National Science Foundation under the award numbers: 1854475 and CAREER-1905103. The authors are also grateful for the useful discussion with Carlos Martínez-Bazán and Charles Meneveau. Declaration of Interests: The authors report no conflict of interest.

* Corresponding author.
E-mail address: rui.ni@jhu.edu (R. Ni).

https://doi.org/10.1016/j.ijmultiphaseflow.2020.103397
0301-9322/

to daughter bubble size distribution, bubble size spectrum has also been extracted from plunging breakers in the context of breaking waves, in which a large volume of gas was entrained as a wave crest plunging into the water and subsequently fragmented into smaller bubbles following a particular size spectrum (Deane and Stokes, 2002; Rojas and Loewen, 2007; Blenkinsopp and Chaplin, 2010). The evolution of bubble size spectrum has also been studied by Martínez-Bazán et al. (1999a) in a high-speed water jet. In these flow environments, bubble breakup was linked to the turbulence characteristics, which was assumed to be *locally* homogeneous and isotropic to invoke the Kolmogorov theory (Kolmogorov, 1941), even though most experiments were not conducted in a condition that strictly follows such an assumption.

The objective of this work is to collect bubble breakup statistics in an experimental facility that follows the homogeneous and isotropic condition in a large area and develop a breakup model completely relying on the available experimental constraints including both ours and other published experimental results. In Section 2, the population balance equation and some typical phenomenological models for daughter bubble size distribution and breakup frequency are reviewed. In Section 3, a new facility that has been designed to study bubble breakup in homogeneous and isotropic turbulence (HIT) is introduced. Section 4 summarizes a number of experimental constraints, including direct measurements (Section 4.1), scaling law of bubble size spectrum for large (Section 4.3) and small (Section 4.4) bubbles, and the convergence time to reach a dynamic equilibrium (Section 4.5). Finally, based on all the constraints, a new model is proposed in Section 4.7. Section 5 summarizes the paper and presents important remarks.

2. Breakup models

2.1. The population balance equation

The time evolution of the number density for bubbles of a certain size D at a given position $\boldsymbol{x}$ and time t, $n(D, \boldsymbol{x}, t)$, can be statistically described by the population balance equation, which is first proposed by Williams (1985):

$$\frac{\partial n}{\partial t} + \nabla\cdot(\boldsymbol{v}n) = -\frac{\partial}{\partial D}(Rn) + \dot{Q}_b + \dot{Q}_c \tag{1}$$

where $\boldsymbol{v}(D, \boldsymbol{x}, t)$ is the advection velocity of bubbles, $R = dD/dt$ is the rate of change of bubble size due to mass dissolution, and $\dot{Q}_b$ and $\dot{Q}_c$ are the rate of change of bubble number density $n(D, \boldsymbol{x}, t)$ due to breakup and coalescence, respectively. For a system that has a very low bubble concentration and negligible dissolution, which is exactly the case for our study, $\dot{Q}_c$ and the dissolution term $\partial(Rn)/\partial D$ can be neglected. By only considering breakup (Martínez-Bazán et al., 2010), Eq. (1) can be re-written as:

$$\begin{aligned}\frac{Dn(D)}{Dt} &\equiv \frac{\partial n(D)}{\partial t} + \nabla\cdot[\boldsymbol{v}n(D)] \\ &= \int_D^\infty m(D_0) f(D; D_0) g(D_0) n(D_0) dD_0 \\ &\quad - g(D)n(D)\end{aligned} \tag{2}$$

Batchelor, 1956 where the first term on the right side is the source term for the bubbles of size D generated by the breakup of all bubbles of sizes larger than D. $m(D_0)$ is the number of daughter bubbles generated from a mother bubble of size D_0; $f(D; D_0)$ is daughter bubble size distribution (also been referred to as breakup kernel (Wang et al., 2003)) and $g(D)$ is breakup frequency, which represents the rate of breakup for a bubble of size D. Note that $f(D; D_0)$ is a conditional probability density function (PDF) of the daughter bubble size D when the mother bubble size is D_0. It is clear that, in Eq. (2), once $f(D; D_0)$ and $g(D)$ are known, $n(D)$ can be easily integrated numerically given the right initial condition.

$f(D; D_0)$ is then replaced with the non-dimensionalized form, $f_D(D^*) = D_0 f(D; D_0)$, in the rest of the paper, where $D^* = D/D_0$ is the non-dimensionalized daughter bubble diameter. Daughter bubble size distribution can also be expressed as a function of the non-dimensionalized volume:

$$f_D(D^*) = D^{*2} f_V(V^*) \tag{3}$$

where $V^* = V/V_0$ is the ratio of the volume of daughter bubbles V to that mother bubbles V_0. If we assume that two daughter bubbles are always generated from every breakup event (binary breakup, $m = 2$ in Eq. 2) and the volume of bubbles conserves during the breakup, daughter bubbles of volume V^* and of volume $1 - V^*$ should be generated at the same probability. This implies that $f_V(V^*)$ should be symmetric about $V^* = 0.5$. It will be shown later that most breakups follow the binary breakup assumption, and m is fixed at 2 for the rest of the paper.

2.2. Models for daughter bubble size distribution

Many models for $f_V(V^*)$ have been proposed in the past few decades. These models typically fall into one of the three groups (Liao and Lucas, 2009) based on the shape of $f_V(V^*)$: Bell-shape (e.g. Martínez-Bazán et al., 1999b; Han et al., 2011), U-shape (e.g. Tsouris and Tavlarides, 1994; Luo and Svendsen, 1996) and M-shape (e.g. Lehr et al., 2002; Wang et al., 2003; Zhao and Ge, 2007). Some of these models are compiled in Fig. 1(a). It is obvious that no consensus has been reached among these models, and it is challenging for simulations to choose which model to implement.

As shown in Fig. 1(a), Bell-shape models have a high probability of generating two daughter bubbles with similar or equal size ($V^* \approx 0.5$, hereafter referred to as equal-size breakup). One such model is proposed by Martínez-Bazán et al. (1999b) by assuming that the probability to generate a daughter bubble of a specific size is proportional to the product of excess stress of the two daughter bubbles. The excess stress was defined as the difference between turbulent dynamic pressure around the daughter bubble and capillary pressure of the mother bubble. If the excess stress of either one of the daughter bubbles is negative, the probability is set as zero because the turbulent dynamic pressure is not strong enough to overcome the capillary pressure to break the bubble.

Opposing to the Bell-shape models, U-shape models predict that most breakup events will preferentially generate two daughter bubbles with significantly-different sizes: one close to zero ($V^* \approx 0$) together with the other one close to the mother bubble size ($V^* \approx 1$) (hereafter referred to as uneven breakup). One typical example of the U-shape models is proposed by Tsouris and Tavlarides (1994) based on the surface energy increment, which is the difference between the total surface energy before and after breakup $4\sigma\pi D_0^2[D^{*2} + (1 - D^{*3})^{2/3} - 1]$, where σ is the surface tension coefficient. The surface energy increment reaches its maximum for an equal-size breakup and minimum for an uneven breakup. Since it was argued that the probability is inversely proportional to the energy, $f_V(V^*)$ looks like a U shape.

The last group is M-shape models. As shown in Fig. 1(a), the M-shape models have three local minima of probability at $V^* = 0$, 0.5 and 1. An example of the M-shape models is the one proposed by Wang et al. (2003) based on the notion of eddy-bubble collision. This model considered the probability of bubbles colliding with eddies that can meet the following two conditions: (i) the eddy size is smaller or equal to the bubble size; (ii) the eddy has either large kinetic energy to surpass the surface energy increment, or large dynamic pressure to overcome the capillary pressure of the bubble. Moreover, the collision frequency with eddies was modelled inspired by the gas kinetic theory, and the PDF of eddy energy was modeled using an exponential function.

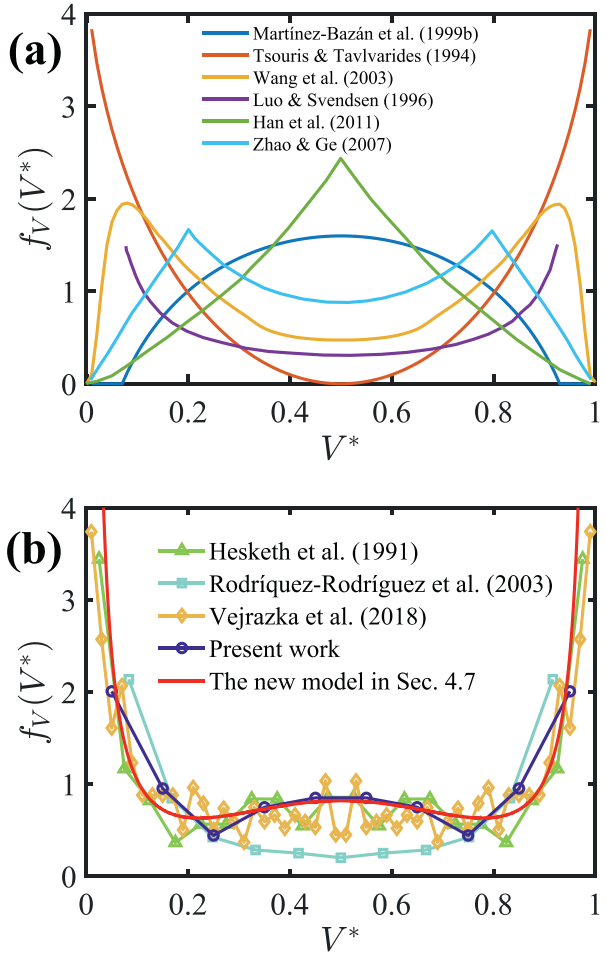

Fig. 1. (a) Daughter bubble size distribution $f_V(V^*)$ versus the non-dimensionalized daughter bubble volume V^* for different proposed models.(b) Daughter bubble size distribution from experiments, including the previous experiments and our experiment (blue circles) as well as the proposed new model (red solid line) in Section 4.7. (For interpretation of the references to colour in this figure legend, the reader is referred to the web version of this article.)

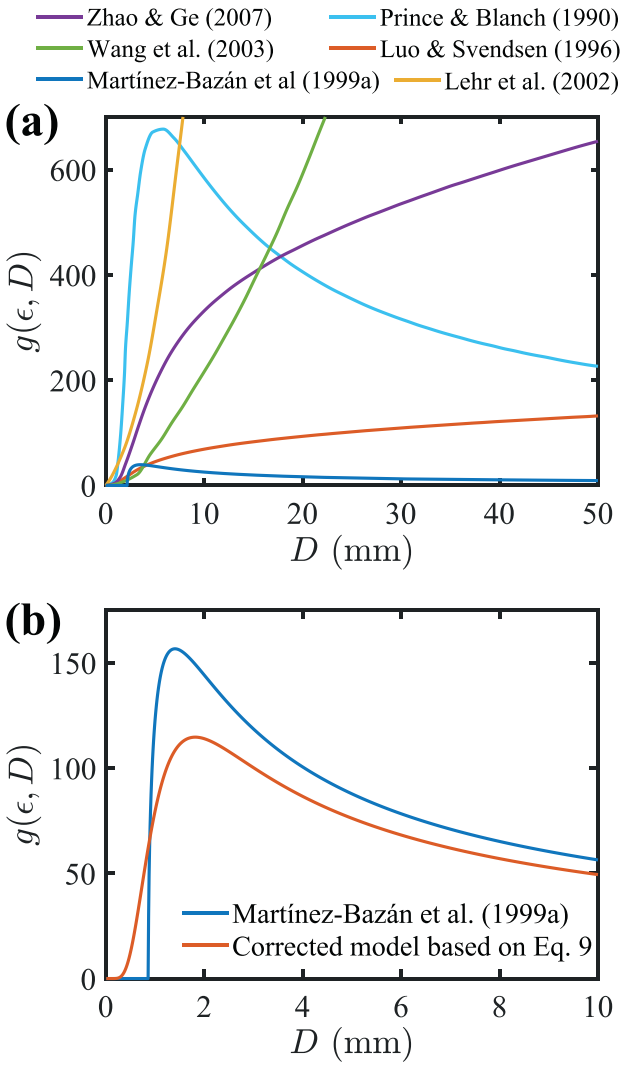

Fig. 2. (a) Breakup frequency versus bubble diameter D for different models. The energy dissipation rate used is $\langle\epsilon\rangle = 5$ m^2/s^3 (b) Comparison of the original breakup frequency model by Martínez-Bazán et al. (1999a) (blue) and the corrected model based on Eq. (9) (red) at $\langle\epsilon\rangle = 50$ m^2/s^3. (For interpretation of the references to colour in this figure legend, the reader is referred to the web version of this article.)

Most of these phenomenological models were proposed based on the argument that daughter bubble size distribution is related to excess energy, stress, and the collision process. As a result, the models also predict that $f_V(V^*)$ should have a strong dependence on both D_0 and the ensemble-averaged turbulent energy dissipation rate $\langle\epsilon\rangle$. Similar to the large variation of $f_V(V^*)$ among different models, the predicted dependences are also inconsistent with one another even qualitatively; $f_V(V^*)$ may increase or decrease as D_0 and $\langle\epsilon\rangle$ change. In addition, the predicted dependences are not supported by the experimental findings, e.g. Rodríguez-Rodríguez et al. (2003) suggested that the dependence is weak. Moreover, many models for $f_V(V^*)$ were not validated in their original paper, whereas some were validated against limited experimental evidence, either by directly comparing with measurements of $f_V(V^*)$ or with the measured bubble size spectrum. For the latter, the calculated bubble size spectrum was obtained by implementing the modeled $f_V(V^*)$ in Eq. (2).

The advantage of using physical arguments in models is clear: (i) it connects to the physical breakup process, (ii) it also predicts the dependence of $f_V(V^*)$ on multiple possible parameters. The downside is equally evident: there are simply too many possible arguments that are available, and they produced very inconsistent results. It poses a formidable challenge for simulations as to which model to implement. In addition, the methodology adopted works like a forward problem, assuming $f_V(V^*)$ based on some breakup mechanisms and hope that the predicted results agree with experiments. The methodology that we are proposing in this paper is the opposite. The question that is being asked here is an inverse problem: what the right features of a correct model for $f_V(V^*)$ should be based on experimental constraints. To address this question, we will summarize some existing experimental results, and use them to derive a new model of $f_V(V^*)$.

2.3. Models for breakup frequency

In addition to $f_V(V^*)$, breakup frequency $g(D)$ is also required to solve the population balance equation. Some of these models proposed by Lee et al. (1987), Prince and Blanch (1990), Tsouris and Tavlarides (1994), Luo and Svendsen (1996), Martínez-Bazán et al. (1999a), Rodríguez-Rodríguez et al. (2003), Lehr et al. (2002), Wang et al. (2003) and Zhao and Ge (2007) are compiled in Fig. 2(a). Similar to $f_V(V^*)$ shown in Fig. 1(a), a large variation of the predicted breakup frequency motivated by different physical mechanisms is observed. One such mechanism

proposed by Martínez-Bazán et al. (1999a) was based on the pressure difference:

$$g(\langle\epsilon\rangle, D) = K_g \frac{\sqrt{\beta(\langle\epsilon\rangle D)^{2/3} - 12\sigma/(\rho D)}}{D} \quad (4)$$

where β is the Kolmogorov constant of the second-order structure function. $\beta = 8.2$ given by Batchelor (1956) was used by Martínez-Bazán et al. (1999a). But a more recent compilation of the Kolmogorov constant (Sreenivasan, 1995; Ni et al., 2013) suggests that this number is closer to $\beta = 7.81$. The prefactor K_g needs to be determined from experiments, which was suggested to be 0.25 by Martínez-Bazán et al. (1999a). For large bubbles, the dynamic pressure, the first term in the square root, dominates, and Eq. (4) can be simplified as $g(\langle\epsilon\rangle, D) = K_g \beta^{1/2} \langle\epsilon\rangle^{1/3} D^{-2/3}$, which suggests that g for large bubbles is proportional to the reciprocal of eddy turn-over time, i.e. $\langle\epsilon\rangle^{-1/3} D^{2/3}$. On the other limit, when the mother bubble size becomes smaller than the critical value, $D_H = (12\sigma/(\beta\rho))^{3/5} \langle\epsilon\rangle^{-2/5}$, breakup frequency will be set as zero, consistent with the argument that bubbles smaller than D_H are simply too strong to be broken. D_H is essentially the Hinze scale (Hinze, 1955).

Similar to models for $f_V(V^*)$, most existing models for breakup frequency were also proposed based on some physical mechanisms. The inconsistency among these models, both quantitatively and qualitatively, points out a problem that there are simply too many possible physical arguments that can lead to drastically different model predictions. In this paper, similar to $f_V(V^*)$, we will take a different approach by constraining the model of $g(\langle\epsilon\rangle, D)$ using experimental results and illustrate the key characteristics that a correct model should encompass.

3. Experimental setup

3.1. V-ONSET vertical water tunnel

Since most models developed for describing bubble breakup rely on an assumption of HIT, it is important to maintain HIT in a large area that the statistics can be collected. Flow configurations adopted include turbulent pipe flow (Hesketh et al., 1991) and turbulent jet (Martínez-Bazán et al., 1999b), neither of which, strictly speaking, can be claimed to be HIT and both of which exhibit some strong spatial velocity gradients that could complicate the results.

A new vertical water tunnel, V-ONSET (Vertical Octagonal Noncorrosive Stirred Energetic Turbulence) (Masuk et al., 2019b), was constructed to study bubble breakup, as shown in Fig. 3(a). This facility has several unique features: (i) The mean flow in the tunnel can be adjusted to keep bubbles in the view area for an extended period of time which allows us to record more breakup events. (ii) HIT can be maintained over a large area in the test section (~ 10 cm) and is decoupled from the mean flow. (iii) There is an octagonal test section in the system that allows for six high-speed cameras imaging deforming and breaking bubbles from views that cover the entire perimeter of the test section. A typical arrangement of the cameras used in this work is shown in Fig. 3(b).

Turbulence in the test section was generated by 88 water jets with the highest speed up to 12 m/s. The jet nozzle diameter is 5 mm. These water jets were fired randomly into the test section to avoid any secondary flows which is key to maintain HIT over a large region. On average, 12.5% of the jets were fired at a time (Variano et al., 2004), and the resulting $\langle\epsilon\rangle$ is about 0.52 m^2/s^3 around the bubbles. ϵ was calculated from the local velocity gradient tensor using tracers around bubbles. Note that this level of $\langle\epsilon\rangle$ may appear to be lower than what has been reported in other papers for studying bubble breakup. Even in our system, if we move the view area closer to the jet array, $\langle\epsilon\rangle$ of 10–1000 m^2/s^3 can be reached. But close to the jet array, like in other works using jets,

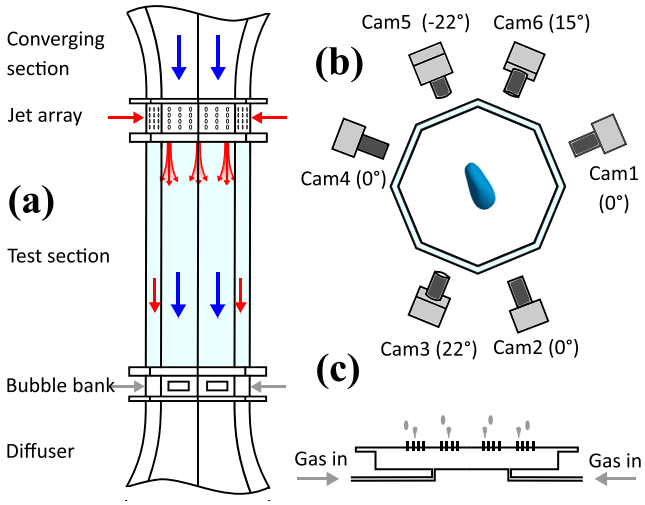

Fig. 3. (a) Schematic of the V-ONSET vertical water tunnel. (b) Top view of six cameras with their respective inclination angles to the horizontal plane. (c) Schematic of the bubble bank located at the bottom of the test section for injecting bubbles.

the spatial gradients of both mean and fluctuation flow velocity are large. Their contributions to the bubble breakup could be as strong as, if not stronger than, the turbulence's, which could potentially complicate how we interpret the results.

Bubbles in V-ONSET were generated at the bottom of the test section from a bubble bank that consists of arrays of hypodermic needles of two different sizes, as shown in Fig. 3(c). Bubbles generated by these needles range from 1 to 10 mm in diameter. The bubble bank is located far below the test section to make sure that bubbles enter the test section with no memory of the injection mechanism so that all breakup events in the test section can be ascribed only to bubble-turbulence interaction. In another study, we analyzed the information of high-concentration of tracer particles around each bubble, which helps us to quantify the Weber numbers based on the horizontal slip velocity and velocity gradient. It has been shown in our case that the mean Weber number for breaking bubbles is about 20–40, which is much larger than the Weber number for all bubbles that are close to one. This suggests that the bubble breakup is indeed dominated by turbulence instead of buoyancy.

3.2. 3D reconstruction of bubble breakup

In most previous works, bubble breakup was identified by using 2D images from one high-speed camera. If a bubble pinches and breaks within the camera 2D plane, the breakup can be observed accurately. However, if this process occurs along a direction that is perpendicular to the 2D plane, which is possible if the flow is truly isotropic, just one view may not suffice.

Here, to provide the 3D reconstruction of the entire breakup process, six synchronized high-speed cameras with one megapixel resolution working at 4000 fps were distributed around the perimeter of the test section to cover the view volume from different angles. A designated LED panel for each camera provided diffused light to cast shadows of bubbles onto camera's imaging plane, from which the bubble silhouette can be extracted. The bubble shape was reconstructed using a new virtual-camera visual hull (VC) method (Masuk et al., 2019a) by enforcing the minimal surface energy criteria.

In the classical limited-angle visual hull (VH) method, the 3D volume of the object is reconstructed by calculating the intersection of the cone-like volume extruded from the silhouette on each camera. Although this method has been used extensively in many

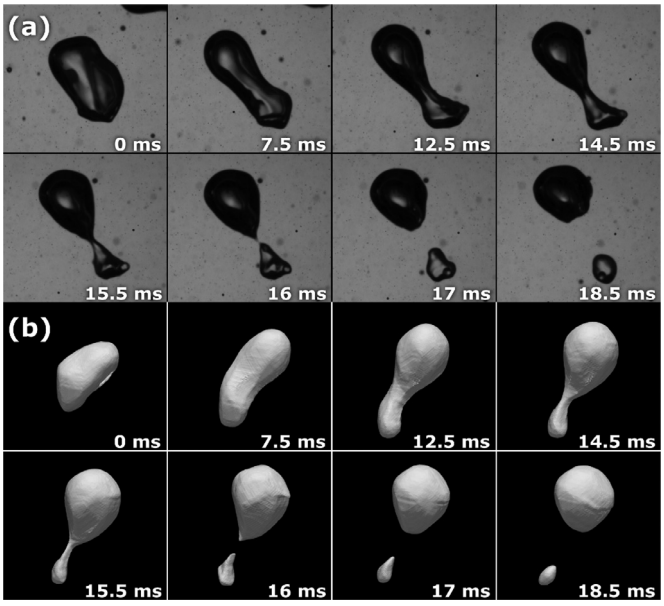

Fig. 4. Example of a bubble breakup event, including (a) raw images on one camera, and (b) 3D reconstructed result of the same bubble. The diameter of an equivalent sphere for this bubble is 2.82 mm.

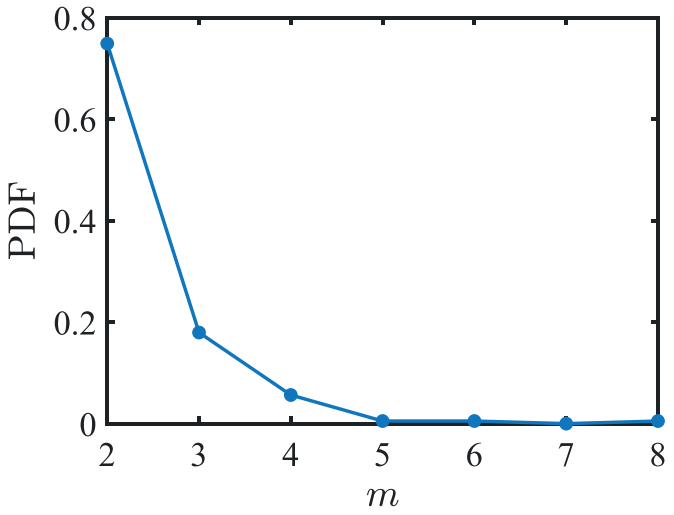

Fig. 5. The distribution of the number of daughter bubbles m produced in each breakup event.

studies (Laurentini, 1994; Matusik et al., 2000; Kutulakos and Seitz, 2000; Mulayim et al., 2003), the VH method tends to overestimate the reconstructed volume if only limited views are provided, which is the case considering the four-camera configuration used in a typical 3D volumetric velocity measurements.

To address this problem, two solutions have been put forward. The first one is simply to acquire more high-speed cameras. Six high-speed cameras were utilized for this purpose. With these many cameras, for almost all breakup events, no matter along which direction the necking process occurs, at least one camera will capture that. The other solution is to enforce a physical constraint, i.e. minimal surface energy, in 3D reconstruction. The limited-angle VH method typically results in sharp corners, but bubbles or droplets do not have very sharp corners due to the surface tension. To implement this constraint, the initial 3D reconstruction was first performed using the standard VH method. This geometry was then projected to many directions where actual cameras were not available, thus the name, virtual camera. Silhouettes on virtual cameras were smoothed iteratively to remove corners with a large curvature, and the smoothed image was integrated into reconstruction again as a new virtual camera to refine the geometry. The refined volume was re-projected back onto actual cameras to make sure the refined geometry was not over-corrected to affect images on actual cameras. Additional details of validating this method by using standard and experimental geometries can be found in Masuk et al. (2019a).

By applying this method to our experiments, deformation and breakup of each bubble can be reliably reconstructed. Fig. 4 shows one typical breakup event imaged by the camera and reconstructed using VC method. The entire process from the initial weak deformation to the final breakup takes about 17 ms, which is 12.1 times of the Kolmogorov time scale (1.4 ms) and 1.5 times of the natural oscillation period of this bubble (11.3 ms, based on Lamb mode 2 bubble natural frequency (Lamb, 1932)). In particular, it can be seen that the daughter bubble size from 2D images appears to be slightly larger than that in the 3D view because the daughter bubble was flattened within the camera 2D plane during the breakup process. This suggests that, if only one camera was used, the daughter bubble size cannot be reliably determined. Therefore, in our setup, the 3D reconstruction was performed for every breakup event, from which daughter bubble size distribution was extracted.

4. Discussion

4.1. Measurement of daughter bubble size distribution

In V-ONSET, the mean turbulent energy dissipation rate was maintained at around 0.52 m^2/s^2. The Reynolds number is defined as $Re = u'L/\nu$, where u' is the fluctuation velocity and L is the integral length scale. Re in our experiments was kept roughly the same at 8000 with $u' = 0.25$ m/s and $L = 3.2$ cm. To measure the daughter bubble size distribution, 190 datasets were collected, and 480,329 bubbles were reconstructed and tracked over time. The majority of these bubbles did not break in the finite residence time that they spent in the view volume. As a result, 195 breakup events were identified, which is more than the work conducted by Hesketh et al. (1991) (used extensively for model validation) but fewer compared with more recent work by Vejražka et al. (2018). Details of these experiments are shown in Table 1. Note that the number of breakup events in our experiments can be enhanced significantly if (i) the bubble injection point is very close to the interrogation window and (ii) the interrogation window is close to the jet array. But we chose to keep the interrogation volume far away from both the bubble injection and the jet array to avoid possible contamination either due to the memory of injection or the inhomogeneity or anisotropy of the flow. Having a small number of breakup events is a compromise to ensure that bubbles break only by intermittent turbulence, not by mean gradients or by bubble injection mechanisms.

Fig. 5 shows the distribution of the number of daughter bubbles identified after each breakup. Note that this number is sensitive to the spatial and temporal resolution. The spatial resolution has to be large enough to resolve even the smallest daughter bubbles, and the temporal resolution needs to be high to avoid mistreating two consecutive binary breakups as one ternary breakup. The smallest bubble size that the current setup can resolve is about 200 μm. The frame rate used to track bubbles is 4000 fps, and each individual breakup event is identified within one frame (0.25 ms). Under this condition, 74.9% of the breakup events are binary ($m = 2$ in Eq. (2)), as shown in Fig. 5. This suggests that the binary bubble indeed dominates the statistics, and only this subset of the dataset

Table 1
Parameters of the existing experiments on daughter bubble size distribution; $\langle\epsilon\rangle$ is turbulent energy dissipation rate, N_b is the number of breakup events, η_k is the Kolmogorov length scale, and D_0 is the mother bubble size. The definitions of *Re* are different based on specific flow configurations used, including jet Reynolds number in Rodríguez-Rodríguez et al. (2003) and Vejražka et al. (2018); and hydraulic-diameter-based Reynolds number in Hesketh et al. (1991). In our work, the Reynolds number is defined in Section 4.1.

	$\langle\epsilon\rangle$ (m^2/s^2)	N_b	*Re*	η_k (μm)	D_0 (mm)
Hesketh et al. (1991)	-	56	1.5×10^5	-	2.7–4.1
Rodríguez-Rodríguez et al. (2003)	12–129	-	3.5×10^3–7×10^4	9.4–17.0	0.7–3.3
Vejražka et al. (2018)	0.01–300	1100	6×10^3–2.6×10^4	7.6–100.0	1.8–5.0
Present work	0.52	195	8×10^3	37.6–50.0	2.9–7.6

will be used in this paper to constrain daughter bubble size distribution.

The daughter bubble size distribution measured from our experiments is shown in Fig. 1(b) as blue dots. The distribution seems to follow a W-shape with a large probability close to $V^* = 0$ and 1 and a small hump close to $V^* = 0.5$. In addition to our experimental results, a limited number of experimental results of $f_V(V^*)$ have been reported in different flow configurations: horizontal two-phase pipe flows (Hesketh et al., 1991), turbulent jets (Rodríguez-Rodríguez et al., 2003), and flows driven by a downward jet array (Vejražka et al., 2018). Details of these experiments are shown in Table 1 for comparison, and the data of $f_V(V^*)$ is shown in Fig. 1(b). Despite the distinct conditions used in different experiments, all experimental results agree quite well with one another for $V^* < 0.2$ or $V^* > 0.8$. A similar hump near $V^* = 0.5$ corresponding to two equal-size daughter bubbles can also be observed in works by Hesketh (1987) and Vejražka et al. (2018).

Models of $f_V(V^*)$ that were introduced in Section 2 are complied in Fig. 1(a). As one can clearly see, in contrast to the nice agreement among experimental results, there is no consensus as to which model to use for bubble breakup. All these models that have been introduced based on some physical arguments do not seem to agree with the experimental results, some of which are closer, such as the U-shaped models. It is our goal of introducing a model, instead of relying on physical arguments, to focus on being constrained by experimental results. However, it is not that straightforward as a W-shaped curve can be fitted with many different functional forms. Therefore, direct measurement alone is not enough, statistics from other experiments will be sought to provide additional constraints.

4.2. Bubble size spectrum and scaling

One such additional experimental constraint is the bubble size spectrum, which quantifies the distribution of bubble size after a series of breakup events. But evaluating the bubble size spectrum is sensitive to how bubbles are introduced in turbulence, whether bubbles are injected once or continuously into the system.

The experimental datasets that can be used include the works by Deane and Stokes (2002), Rojas and Loewen (2007), and Blenkinsopp and Chaplin (2010), all of which reported bubble size spectrum produced during air entrainment and fragmentation in breaking waves, as shown in Fig. 6(a). As wave plunges back into the pool, it traps a large cavity of gas, which subsequently breaks into a swarm of small bubbles by turbulence. The bubble size spectrum is therefore produced via the bubble cascade process. Similar to the Richardson turbulence cascade, large bubbles break into smaller ones and so on until bubble size drops to the Hinze scale, where the surface tension becomes too strong for bubbles to be broken by turbulence. In the work by Deane and Stokes (2002), the experiment was conducted in a seawater wave plume with plunging breakers generated by a wave paddle on one side of the flume. In this experiment, two distinct scaling laws separated by the Hinze scale were observed, as shown in Fig. 6(a). For super-Hinze bubbles ($D > D_H$), the number density exhibited $D^{-10/3}$, whereas a different scaling law $n(D) \propto D^{-3/2}$ was observed for sub-Hinze-scale bubbles ($D < D_H$).

In the dimensional analysis conducted in the same paper, a quantity called the average rate of air supply was introduced to represent the normalized volume of gas entrained in water per unit time, which indicates that large bubbles are continuously introduced into the control volume at a relatively constant rate over this time period. Once the breakup rate and birth rate of bubbles at each size become close to each other, the bubble size spectrum will remain unchanged. This case is referred to as, *continuous injection*, to suggest that a constant bubble injection at large sizes is maintained.

Martínez-Bazán et al. (1999a) measured the bubble size spectrum by injecting air bubbles using a needle with a diameter of 0.394 mm into a fully-developed turbulent jet. The Reynolds number based on the exit velocity and equivalent nozzle diameter for the jet was kept at 51,000. Subjected to strong turbulence, bubbles break into smaller and smaller sizes as they continuously move downstream following the mean flow. Since the interrogation window is moving downstream with bubbles and away from the injection point, the measured bubble size spectrum, rather than reaching an equilibrium state, keeps shifting towards smaller sizes, as shown in Fig. 6(b). This entire experiment is essentially the same as injecting large bubbles only *once* into a fixed control volume at the beginning of an experiment and observing the change of bubble size spectrum over time, which is referred to as *one-time injection* hereafter. The spatial evolution of $n(D)$ as a function of the distance between the interrogation window to the nozzle exit X is converted to the temporal evolution as a function of T, where T is the time for a bubble to travel from the nozzle exit to X following the mean flow.

Superposing bubble size spectra at different times from the *one-time injection* experiments provides a reasonable estimation of the equilibrium bubble spectrum in the *continuous injection* case. The solid red line in Fig. 6(b) shows the result of superposing data from different X (or equivalently T) together to approximate the bubble spectrum from *continuous injection*. Even with only five different T, the superposed spectrum seems to exhibit a similar -10/3 power law for a range of bubble sizes near $D = 1$ mm, which is consistent with the work by Deane and Stokes (2002). For this particular experiment, given the limitation of the camera resolution, the scaling for the sub-Hinze range cannot be measured accurately.

4.3. Super-Hinze-scale bubble spectrum

For super-Hinze-scale bubbles ($D > D_H$), it seems that experiments conducted in different configurations all suggest the possible existence of $-10/3$ scaling law: $n(D) \propto D^{-10/3}$. It indicates that this scaling may be universal for bubble breakup in turbulence as long as bubbles are *continuously* injected at large sizes. In this section, we intend to see if we can use this scaling law to constrain breakup models.

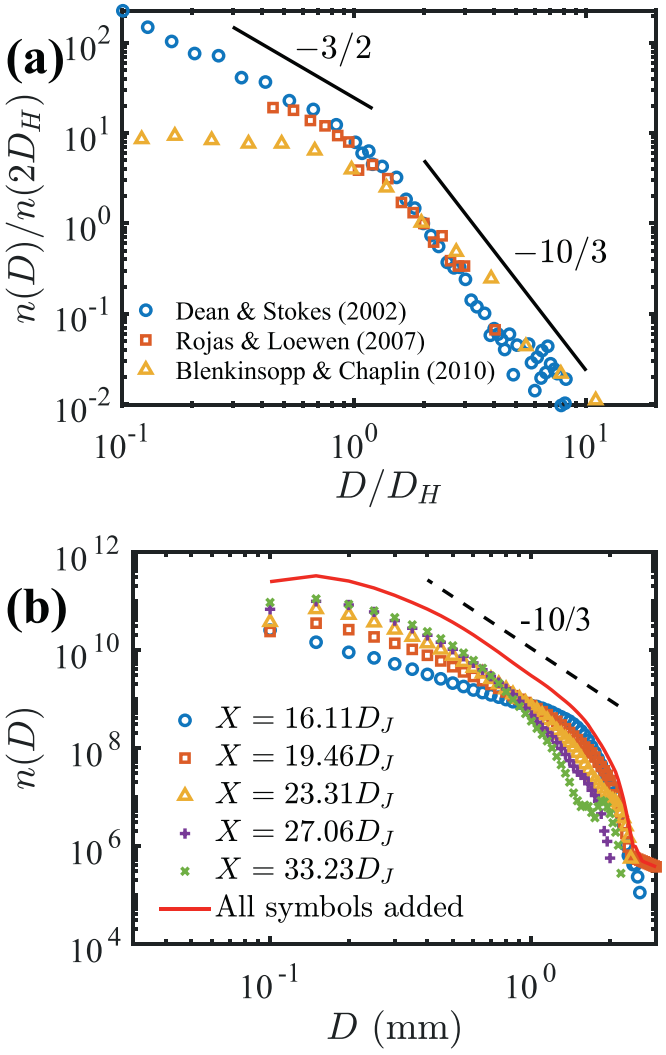

Fig. 6. (a) Bubble size spectrum $n(D)$ versus bubble diameter D from wave-breaking experiments (Deane and Stokes, 2002; Rojas and Loewen, 2007; Blenkinsopp and Chaplin, 2010). Solid lines show the two scaling laws proposed in the paper by Deane and Stokes (2002). Note that D is normalized by the corresponding Hinze scale D_H in each experiment, and $n(D)$ is divided by $n(D = 2D_H)$.(b) The evolution of bubble size spectrum as a function of the distance between the measurement window to the nozzle exit X normalized by the nozzle diameter D_J (Martínez-Bazán et al., 1999b). The red solid line indicates the superposition of all X and the black dashed line shows the -10/3 scaling law. (For interpretation of the references to colour in this figure legend, the reader is referred to the web version of this article.)

Following the conditions of *continuous injection*, in the model, we assume that (i) bubbles with the largest size are continuously fed into the system at a constant rate; (ii) when a large mother bubble of size D_0 breaks, it generates m identical-sized daughter bubbles with a diameter of $m^{-1/3}D_0$ due to volume conservation. m can be any number; (iii) The system reaches a dynamic equilibrium when the birth rate balances with the breakup rate for bubbles of any sizes.; (iv) Bubble breakup frequency follows Eq. (4). The breakup frequency for both mother bubbles D_0 and daughter bubbles $m^{-1/3}D_0$ ($D_0 > D_H$ and $m^{-1/3}D_0 > D_H$) can be expressed approximately as $\langle\epsilon\rangle^{1/3}D_0^{-2/3}$ and $\langle\epsilon\rangle^{1/3}(m^{-1/3}D_0)^{-2/3}$ respectively.

Since all the daughter bubbles of size $m^{-1/3}D_0$ are generated from breakup events of the mother bubbles of size D_0, the birth rate of the daughter bubbles is: $N_1 m\langle\epsilon\rangle^{1/3}D_0^{-2/3}$, where N_1 is the total number of the mother bubbles. If the number of the daughter bubbles of diameter $m^{-1/3}D_0$ is denoted as N_2, the breakup rate of these daughter bubbles is: $N_2\langle\epsilon\rangle^{1/3}(m^{-1/3}D_0)^{-2/3}$. Finally, the dynamical equilibrium yields a simple relationship between N_1 and N_2:

$$N_1 m\langle\epsilon\rangle^{1/3}D_0^{-2/3} = N_2\langle\epsilon\rangle^{1/3}(m^{-1/3}D_0)^{-2/3} \quad (5)$$

Rearrange Eq. (5) yields $N_2 = m^{7/9}N_1$. The total number of mother and daughter bubbles can also be expressed as $N_1 = n_1 d(D_0)$ and $N_2 = n_2 d(m^{-1/3}D_0)$, where n_1 and n_2 are the number density of mother bubbles and daughter bubbles, respectively, $d(D_0)$ and $d(m^{-1/3}D_0)$ are the corresponding bin sizes. By substituting N_1 and N_2 in Eq. $N_2 = m^{7/9}N_1$ with n_1 and n_2, the relationship $n_2(m^{-1/3}D_0) = m^{10/9}n_1(D_0)$ can be obtained. For the equation to hold, $n(D) \sim D^{-10/3}$.

In the discussion above, the power law of super-Hinze-scale bubbles directly comes from the fact that breakup frequency is proportional to $D^{-2/3}$, which seems to suggest that breakup frequency, rather than daughter bubble size distribution, dominates the bubble size spectrum, at least for super-Hinze-scale bubbles considered.

This simple analytical model was originally proposed by Garrett et al. (2000) to explain the scaling law of bubble size spectrum observed in breaking waves. This model assumes a delta function in the daughter bubble size distribution, $f_V(V^*)$. To account for different models proposed for $f_V(V^*)$, we also solved the population balance equation (Eq. (2)) using two different models proposed by Martínez-Bazán et al. (1999b) (equal-size breakup, Bell-shape) and Tsouris and Tavlarides (1994) (uneven breakup, U-shape). As shown in Fig. 1(a), these two models have a nearly opposite prediction of daughter bubble size distribution. Since the mean flow will only transport bubbles without affecting breakup processes, the convective term in Eq. (2) was neglected. Eq. (2) is then integrated in time on a linear grid using the 1^{st}-order forward Euler method. The grid size and time step were set at $\Delta D = 0.1$ mm and $\Delta t = 3 \times 10^{-5}$ s respectively considering the numerical precision and computational cost. The initial condition of $n(D)$ was set as zero for bubbles of all D. At each time step, a constant number density was added to the bin of $D = 10$ mm to maintain a constant injection rate, and $\langle\epsilon\rangle$ is set as 50 m^2/s^3. The simulation continued until the scaling of the large bubbles stopped changing.

Fig. 7 shows the time evolution of bubble size spectrum. After reaching the dynamical equilibrium, bubble size spectra calculated by implementing two different models exhibit the same -10/3 power law for super-Hinze-scale bubbles. This observation confirms the conjecture that the scaling law for super-Hinze-scale bubbles is determined solely by breakup frequency, rather than by daughter bubble size distribution. In fact, if we assume that breakup frequency follows a power law, $g(D) \sim D^{\gamma}$ (the exponent γ depends on a specific model), bubble size spectrum can be written as: $n(D) \sim D^{-4-\gamma}$ based on Eq. (5). It implies that the equilibrium bubble size spectrum, at least for super-Hinze-scale bubbles, can only be used to constrain models of breakup frequency, not daughter bubble size distribution.

The observed -10/3 scaling law for super-Hinze-scale bubble size spectrum from at least four experimental results (Deane and Stokes, 2002; Rojas and Loewen, 2007; Blenkinsopp and Chaplin, 2010; Martínez-Bazán et al., 1999b) provides a strong experimental constraint that the breakup frequency should exhibit $g \propto D^{-2/3}$ for large bubbles. This result agrees with the model by Martínez-Bazán et al. (1999b), which will be used for the rest of this paper.

4.4. Sub-Hinze-scale bubble spectrum

The sub-Hinze-scale bubble scaling could also be used to constrain the models of daughter bubble size distribution. Here, we investigate what characteristics of $f_V(V^*)$ could potentially affect the scaling for sub-Hinze-scale bubbles.

As the bubble size drops below the Hinze scale, bubbles will remain spherical and difficult to break because of the strong surface tension. This argument implies that: (i) Unlike super-Hinze-scale bubbles, the scaling law observed for sub-Hinze-scale bubbles should not be determined by the breakup frequency because there is no cascade process in this regime; (ii) Most sub-Hinze-scale bubbles are produced primarily by the breakup of super-Hinze-scale bubbles.

Moreover, this sub-Hinze scaling should be determined by bubbles with size slightly larger than the Hinze scale $D \gtrsim D_H$ rather than by the extremely large ones $D \gg D_H$. First of all, these extremely large bubbles are rare, orders of magnitude fewer than the ones close to the Hinze scale, as shown in Fig. 6(a). Even though they can produce small sub-Hinze-scale bubbles, the number that can be generated is small. Second, in the previous section, it was shown that breakup frequency drops as bubble size grows, which indicates that very large bubbles on average take longer to break even though they may break in a more violent manner. Since the number of breakup events per unit time is proportional to the product of the number of bubbles and breakup frequency, it is reasonable to conclude that most sub-Hinze-scale bubbles are generated by bubbles slightly larger than the Hinze scale.

Following these arguments, assuming many bubbles with an identical size D_H all break at once, the resulting sub-Hinze-scale bubble size spectrum $n(D)$ should be equal to daughter bubble size distribution $f_D(D^*)$. As $n(D)$ seems to exhibit a scaling law for sub-Hinze-scale bubbles, we assume a power law for $f_D(D^*)$ as $D^* \to 0$, i.e. $f_D(D^*) \sim D^{*\alpha}$ (or equivalent $f_V(V^*) \sim V^{*(\alpha-2)/3}$ based on Eq. 3), where α is the exponent that needs to be determined. The experimental result by Deane and Stokes (2002) has shown that $n(D) \sim D^{-3/2}$ for $D < D_H$, which suggests that the scaling exponent α for $f_D(D)$ should be a negative constant i.e. -3/2.

This relationship of $f_D(D^*) \sim D^{*-3/2}$ (or equivalent $f_V(V^*) \sim V^{*-7/6}$) hinges on an assumption that the entire sub-Hinze-scale bubble spectrum is contributed by bubbles at one particular size around the Hinze scale D_H. In practice, a range of super-Hinze-scale bubbles can all produce sub-Hinze-scale bubbles after breakups, and this effect is taken into account numerically by conducting a similar simulation as what has been performed in Section 4.3. We found that the exponent α has to be corrected to -2 (or equivalent $f_V(V^*) \sim V^{*-4/3}$) to reflect this broadband contribution. The new model can be expressed as:

$$f_V(V^*) = \frac{V^{*-4/3} + (1-V^*)^{-4/3}}{\int_{V^*_{min}}^{V^*_{max}} [V^{*-4/3} + (1-V^*)^{-4/3}] dV^*} \tag{6}$$

In addition to $V^{*-4/3}$, the other term $(1-V^*)^{-4/3}$ is introduced to satisfy the volume-conservation requirement. This term becomes negligible compared with $V^{*-4/3}$ as V^* approaches zero for very small daughter bubbles. Therefore, this new model of $f_V(V^*)$ still satisfies the power-law relationship in the limit $f_V(V^*) \sim V^{*-4/3}$ for $V^* \to 0$ (or equivalent $f_D(D^*) \sim D^{*-2}$ for $D^* \to 0$).

$V^*_{\min}$ ($V^*_{\max} = 1 - V^*_{\min}$) is the cutoff close to $V^* = 0$ (or $V^* = 1$) to avoid generating arbitrarily small daughter bubbles, which would not be physical. Such a cutoff is also necessary for experimental results shown in Fig. 1(a) because $f_V(V^*)$ has to drop to zero for very small V^*. In addition, the cutoffs were also introduced in many other models, such as the ones by Martínez-Bazán et al. (1999b), Tsouris and Tavlarides (1994), Luo and Svendsen (1996).

This new model in Eq. (6) is then numerically implemented in the population balance equation following the same procedure as described in Section 4.3. The time evolution of bubble size spectrum is shown in Fig. 8(a). Compared with previous models shown in Fig. 7(a) and (b), although the proposed new model of $f_V(V^*)$ reaches the same -10/3 scaling law for super-Hinze-scale bubbles,

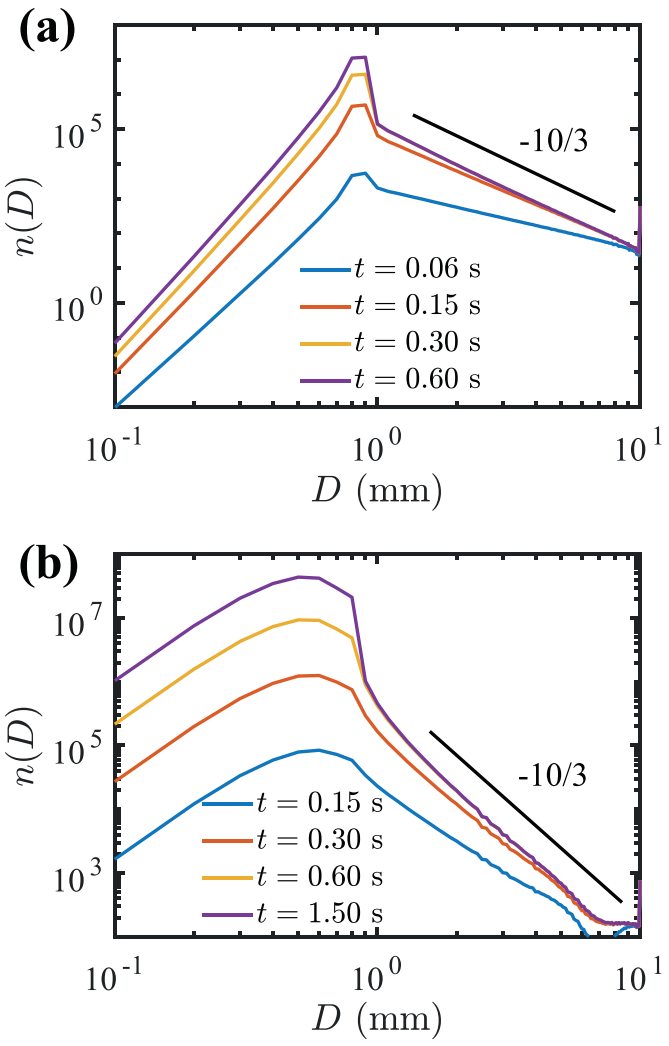

Fig. 7. Time evolution of bubble size spectrum $n(D)$ versus bubble size D obtained from numerically solving Eq. 2 with different models for daughter bubble size distribution: (a) Martínez-Bazán et al. (1999b) and (b) Tsouris and Tavlarides (1994). The simulation was performed by injecting the largest bubbles of 10 mm in size at a constant rate in turbulence with $\langle \epsilon \rangle = 50$ m^2/s^3.

it shows a distinct negative -3/2 exponent, rather than a positive exponent in previous models, for the sub-Hinze scaling law range.

Note that the scaling exponent for sub-Hinze-scale bubbles reported in different works is not exactly the same. Deike et al. (2016) summarized several experiments on breaking waves (Deane and Stokes, 2002; Rojas and Loewen, 2007; Blenkinsopp and Chaplin, 2010), in which a wide range of scaling exponents have been reported. More recently, simulations on breaking waves (Wang et al., 2016; Chan et al., 2018) and bubbles entrained in strong free-surface turbulence (Yu et al., 2020) suggested that this scaling exponent could range from -3 to -4/3. Although there is no consensus on the exact value of this exponent, most prior works suggested that this exponent is likely to be a negative number. Here, we used the most cited work by Deane and Stokes (2002) to constrain $f_V(V^*)$ as V^* approaches zero. In addition, the cutoff used in Eq. (6) does affect the final scaling exponent of sub-Hinze-scale bubbles. The exponent changes from -3/2 to -1.2 as the cutoff increases by an order of magnitude. It suggests that the exponent is not very sensitive to the selected cutoff. But this weak dependence still indicates that the observed wide range of scaling exponents reported in experiments could depend on how small the daughter bubbles can be generated during the

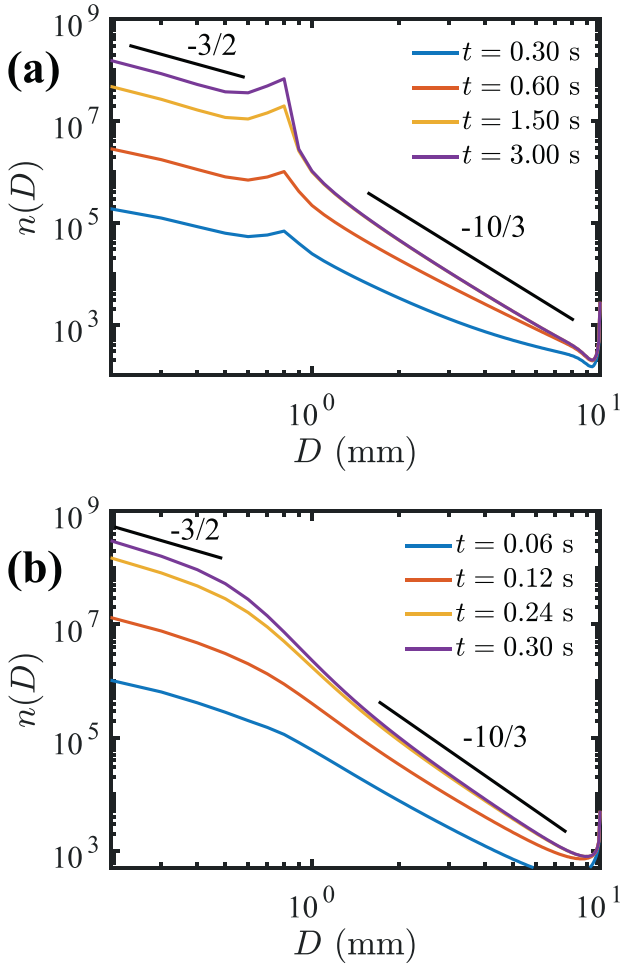

Fig. 8. Time evolution of bubble size spectrum by implementing (a) Eq. (6) for daughter bubble size distribution and Eq. (4) for breakup frequency. (b) Eq. (6) for daughter bubble size distribution and Eq. (9) for corrected breakup frequency after accounting for the log-normal distribution of ϵ. Other conditions remain the same as those employed in Fig. 7. Two scaling laws with respective exponent of -3/2 and -10/3 are shown by two solid lines.

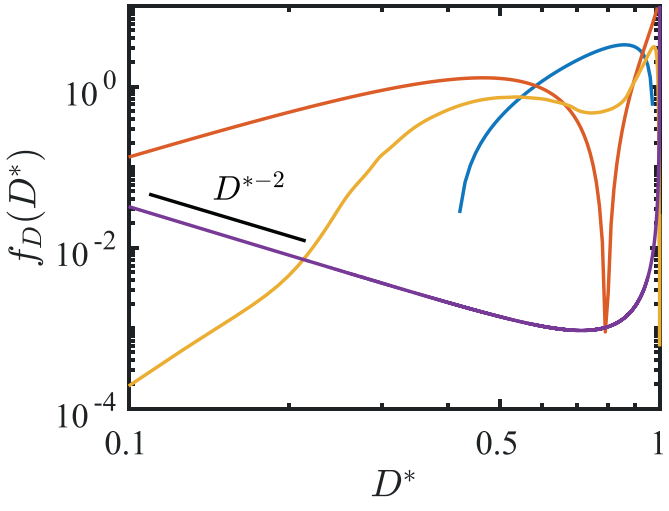

Fig. 9. Daughter bubble size distribution $f_D(D^*)$ versus the non-dimensionalized daughter bubble diameter D^* for different proposed models by Martínez-Bazán et al. (1999b) (blue), Tsouris and Tavlarides (1994) (red), Wang et al. (2003) (yellow) and Eq. (6) (purple). The black solid line indicates the D^{*-2} scaling law near zero. (For interpretation of the references to colour in this figure legend, the reader is referred to the web version of this article.)

breakup process, which could be affected by the surface tension and water contamination.

To examine other models in the limit of $D^* \to 0$, $f_D(D^*)$ from several previous models are shown in Fig. 9 in the logarithmic scale to emphasize the scaling as $D^* \to 0$. Eq. (6) is shown as the purple solid line, which clearly exhibits a power law with a negative exponent of -2 as $D^* \to 0$. Other models seem to suggest the opposite. If a power law is fitted to these models for small D^*, the exponent would be positive, which will not help to generate the sub-Hinze-scale bubble size spectrum with a negative exponent suggested by many experiments.

4.5. Convergence time

As aforementioned in Section 4.3, as the bubble size cascade process continues for *continuous injection*, the super-Hinze-scale bubble size spectrum will eventually converge to the same power law scaling of $D^{-10/3}$, regardless of $f_V(V^*)$, so this scaling law cannot be used to constrain the model of $f_V(V^*)$. However, as shown in Figs. 7 and 8(a), different choices of models for $f_V(V^*)$ affect how long bubble size spectrum reaches the equilibrium state, which is referred to as convergence time (τ_c) hereafter. This result could serve as another constraint to $f_V(V^*)$ for V^* close to 0.5.

As shown in Fig. 7, τ_c for the model by Martínez-Bazán et al. (1999b) is only half of that by Tsouris and Tavlarides (1994). The two models show the opposite trend with respect to V^*: one peaks at $V^* = 0.5$ (equal-size breakup) and the other one peaks at V^* close to 0 and 1 (uneven breakup). To enable a smooth transition between these two limits, a mixed model is introduced:

$$f_V(V^*) = \omega \frac{1 - cos(2\pi V^*)}{\int_0^1 [1 - cos(2\pi V^*)] dV^*} + (1-\omega) \frac{V^{*-4/3} + (1-V^*)^{-4/3}}{\int_{V^*_{min}}^{V^*_{max}} V^{*-4/3} + (1-V^*)^{-4/3} dV^*} \quad (7)$$

where the first term, cosine function, represents a simplified Bell-shape curve that has a higher probability of equal-size breakup, and the second term is from Eq. (6) to represent the U-shape model for uneven breakups. ω is the weight parameter that can be changed smoothly between 0 and 1 to switch between these two shapes.

The weighted-averaged model was implemented in the population balance equation following the procedure in Section 4.3 to obtain the time evolution of bubble size spectrum. The spectra (in the range of $D = 2$–8 mm) at different times were fitted with power laws, from which the scaling exponent β was extracted and plotted versus time. As shown in Fig. 10(a), as the simulation time τ increases, the scaling exponents of super-Hinze-scale bubbles from models with different ω all approach the same number close to -10/3, but it takes longer to reach that asymptotic value for smaller ω. Fig. 10(b) shows τ_c versus ω. Clearly, τ_c for $\omega = 1$ (Bell-shape) is indeed much shorter than the case of $\omega = 0$ (U-shape), which is consistent with what has been observed in Fig. 7. This implies that models with a higher probability of equal-size breakup will converge faster than those with more uneven breakup events.

τ_c seems to approach a constant as ω increases. To estimate this limiting value of τ_c, we assume an extreme case, in which the daughter bubble size distribution is a delta function at $V^* = 0.5$, suggesting that every breakup event will result in two identical-sized daughter bubbles. Performing the same simulation, the shortest convergence time $\tau_{c,\min} = 0.14$ is obtained, which is shown in Fig. 10(b) as a dashed line. It can be seen that this value is very close to the results obtained from the weighted-averaged model

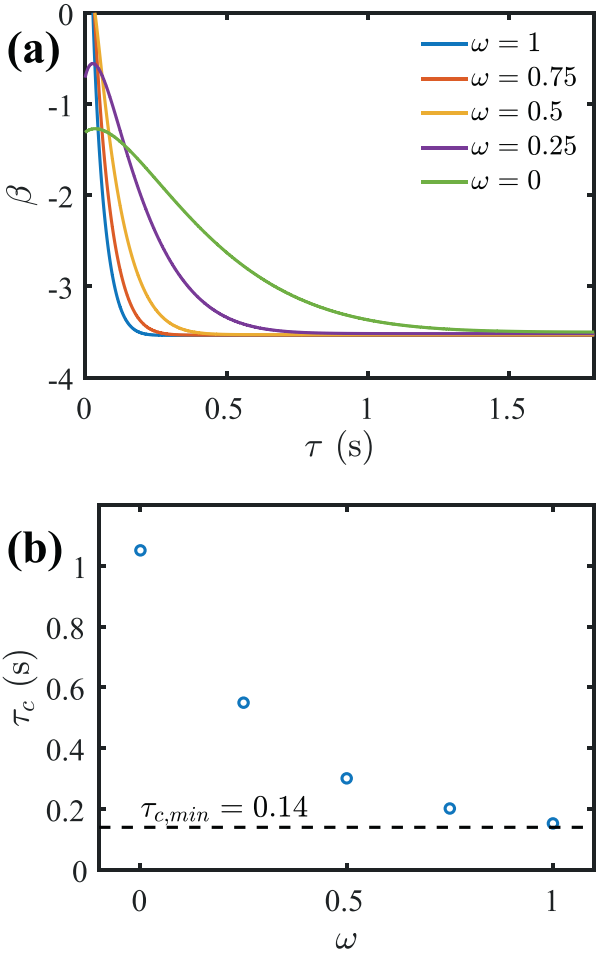

Fig. 10. (a) Time evolution of the scaling exponent β of bubble size spectrum for super-Hinze-scale bubbles ($D > D_H$) for different weight ω used in the mixed model (Eq. (7)). (b) Convergence time τ_c versus ω; The dash line indicates the minimum convergence time $T_{c,min} = 0.14$ by assuming a delta function at $V^* = 0.5$ for daughter bubble size distribution.

with $\omega = 1$. In the opposite extreme ($\omega \to 0$), where every breakup event will result in one daughter bubble with almost the same size to the mother bubble and the other one with size close to zero, the convergence time is infinity.

The question arises as to what the physical meaning of this convergence time is. We conjecture that the scaling law of super-Hinze-scale bubbles reaches its final converged exponent once the largest bubble completes the entire cascade process to reach the Hinze scale. Following this argument, we consider a scenario that a large bubble with a diameter D_1 is injected into turbulence at the very beginning. After time $T_1 = 1/g(\langle\epsilon\rangle, D_1)$, the large bubble breaks into two daughter bubbles of the same size $D_2 = (1/2)^{1/3} D_1$, each one of which will break subsequently after $T_2 = 1/g(\langle\epsilon\rangle, D_2)$. This cascade process continues until all bubbles become equal or smaller than D_H after n iterations. $g(\langle\epsilon\rangle, D_1)$ and $g(\langle\epsilon\rangle, D_2)$ are the breakup frequency of the mother and daughter bubbles, respectively, given by Eq. (4). The cascade time scale is calculated based on $T_1 + T_2 + \cdots + T_n$. For $D_1 = 10$ mm and $\langle\epsilon\rangle = 50$ m^2/s^2 (same with the parameters adopted in Section 4.3), the calculated bubble size cascade time is 0.11 s, which is close to the numerical solution of $\tau_{c,min} = 0.14$ s assuming a delta function for $f_V(V^*)$. This result confirms our conjecture that, for *continuous injection*, the super-Hinze scaling converges when the bubble size cascades from the largest bubbles to bubbles close to the Hinze scale.

In wave-breaking experiments (Deane and Stokes, 2002; Rojas and Loewen, 2007; Blenkinsopp and Chaplin, 2010), only the equilibrium scaling laws were reported; τ_c cannot be determined accurately because the entire process finishes within a short period of time. Therefore, without any experimental results, τ_c, although it guides the model development, cannot be used as a constraint. Nevertheless, τ_c for *continuous injection* is related to how fast bubble size spectrum changes for experiments with *one-time injection* because the equilibrium bubble size distribution for *continuous injection* is equivalent to the superposition of bubble size spectra at different times from *one-time injection*, which will be introduced in Section 4.7 to constrain a proposed new model.

4.6. Breakup frequency correction

From Sections 4.2 to 4.5, three types of possible experimental results, including the super- and sub-Hinze scaling laws and the convergence time, were discussed. Although the implemented model seems to perform well to predict the limiting scaling exponents for bubbles much larger or much smaller than D_H, a small hump near D_H is observed, as shown in Figs. 7 and 8(a). This hump indicates an accumulation of bubbles at this scale, which was not observed in experiments (e.g. Fig. 6(a)).

The accumulation of bubbles at the Hinze scale can be ascribed to the sharp transition of breakup frequency from super-Hinze to sub-Hinze-scale bubbles. As shown in Fig. 2(b), the model proposed by Martínez-Bazán et al. (1999b) shows a peak of the breakup frequency near D_H but drops abruptly at soon as the bubble diameter falls below D_H. This indicates that bubbles slightly larger than D_H break frequently and produce a large number of bubbles near D_H that never break, which leads to the observed accumulation in bubble size spectrum.

The sharp transition of bubble breakup frequency at the Hinze scale can be attributed to the fact that the Hinze scale is defined based on $\langle\epsilon\rangle$ (Hinze, 1955). In turbulence with strong intermittency, the local energy dissipation rate ϵ could be orders of magnitude larger than $\langle\epsilon\rangle$. Therefore, sub-Hinze-scale bubbles, if encountering an eddy with sufficiently large local ϵ, may still break, and thus its breakup frequency may not be zero. The distribution of the local energy dissipation rate ϵ can be modelled base on the Kolmogorov refined theory in 1962 (Kolmogorov, 1962) and multifractal spectrum (Meneveau and Sreenivasan, 1991). In particular, if we consider the energy dissipation rate ϵ coarse-grained at the bubble scale D, i.e. ϵ_D, it follows a log-normal distribution:

$$P(\epsilon_D/\langle\epsilon\rangle) = \frac{1}{\epsilon_D/\langle\epsilon\rangle} \frac{1}{\sqrt{2\pi\,(A + \mu \ln(L/D))}} \cdot \exp\left[-\frac{\left(\ln(\epsilon_D/\langle\epsilon\rangle) + \frac{1}{2}(A + \mu \ln(L/D))\right)^2}{2(A + \mu \ln(L/D))} \right] \tag{8}$$

where $\mu \approx 0.25$ is the intermittency exponent, L is the integral length scale of turbulence and D is the coarse-graining scale over which the local energy dissipation rate is averaged. The offset A represents a large-scale variability of ϵ when $D = L$, which depends on specific flow configurations. Although it may seem that $P(\epsilon_D/\langle\epsilon\rangle)$ depends on bubble size, in our experiments, the dependence seems to be weak as $A \gg \mu \ln(L/D)$. Therefore, for the rest of the discussion, $A + \mu \ln(L/D)$ is assumed to be a constant of 1.2, and ϵ_D is replaced with ϵ hereafter for simplicity.

The expression for breakup frequency considering the distribution of ϵ is then given by

$$g_{corr}(\langle\epsilon\rangle, D) = \int_0^\infty g(\epsilon, D) P(\epsilon/\langle\epsilon\rangle) d(\epsilon/\langle\epsilon\rangle) \tag{9}$$

where $g_{corr}(\langle\epsilon\rangle, D)$ is the corrected breakup frequency. By substituting Eqs. (4) and (8) into Eq. (9), we immediately obtain $g_{corr}(\langle\epsilon\rangle, D)$ for a given mean energy dissipation rate $\langle\epsilon\rangle$. Fig. 2(b) shows the comparison between the original breakup frequency and the corrected one with $\langle\epsilon\rangle$ of 50 m^2/s^2. The corrected breakup frequency shows a smoother transition near D_H. Note that the corrected breakup frequency appears to be lower than the original one, which implies the prefactor K_g in Eq. (4) needs to be adjusted to account for this correction.

The simulation shown in Fig. 8(a) was repeated using Eq. (9). The results are shown in Fig. 8(b). As expected, the hump near D_H is smoothed, while the sub- and super-Hinze-scale bubble scaling remain the same.

4.7. A new model for daughter bubble size distribution

Finally, a new model of daughter bubble size distribution is proposed to satisfy all the experimental constraints discussed in the previous sections. Following the weighted-average model in Eq. (7) and using $\omega = 0.3$ and $V^*_{\min} = 0.02$ as two fitting parameters, the modelled daughter bubble size distribution is shown in Fig. 1(b) to compare with other experiments. The fitted new model appears to agree with experimental measurements, capturing two features: (i) increasing breakup probability as V^* approaches 0 and 1, and (ii) a small hump near $V^* = 0.5$ observed in our results and also by Hesketh et al. (1991) and Vejražka et al. (2018).

The new model will also adopt the formulation of the corrected breakup frequency following Eq. (9) to account for the distribution of local ϵ. For super-Hinze-scale bubbles, as discussed in Section 4.3, the converged scaling is determined by breakup frequency, so if the new model is employed to calculate the final equilibrium bubble size spectrum in a system with *continuous injection*, the scaling exponent will converge to a number close to -10/3.

Sub-Hinze-scale bubbles are only sensitive to the second term in the new model (Eq. (7)) that determines the daughter bubble size distribution at $V^* \gtrsim 0$ or $V^* \lesssim 1$. As discussed in Section 4.4, this formulation should satisfy the criterion to generate a negative scaling exponent for sub-Hinze-scale bubbles. The first term, similar to the Bell-shape model, is added to match with the experimental measurements of $f_V(V^*)$; this term is also important for shortening τ_c for *continuous injection* and accelerate the time evolution of bubble size spectrum for *one-time injection* based on the discussion in Section 4.5.

As a final test, the new model is implemented in Eq. (2) to predict the time (space) evolution of bubble size spectrum with the experimental data provided by Martínez-Bazán et al. (1999a). In the simulation, the unsteady term in Eq. (2) was neglected because the bubble size spectrum does not change over time based on the experiments. Eq. (2) was then integrated in space on a linear grid with size $\Delta D = 0.025$ mm using 1^{st}-order explicit Euler method with $\Delta X = 0.15$ mm. The convective velocity and turbulent energy dissipation rate along the jet centerline were found in Martínez-Bazán et al. (1999a) and Martínez-Bazán (1998). The prefactor K_g in Eq. (4) is set as 0.4 to fit with the experiments. The simulation results of the time (space) evolution of bubble size spectrum are shown in Fig. 11 as solid lines, and the symbols represent the experimental data at different distances X away from the original injection point normalized by the nozzle diameter D_j. $n(D)$ at $X/D_J = 16.11$ was input into the model as the initial condition, and Eq. (2) was integrated over time T (or equivalently over distance X, as discussed in Section 4.2). It is observed that bubble size spectra obtained by the new model agree well with the experimental data for both small and large bubbles.

Finally, it is important to emphasize that the new model (Eq. (7)) did not come from any phenomenological arguments,

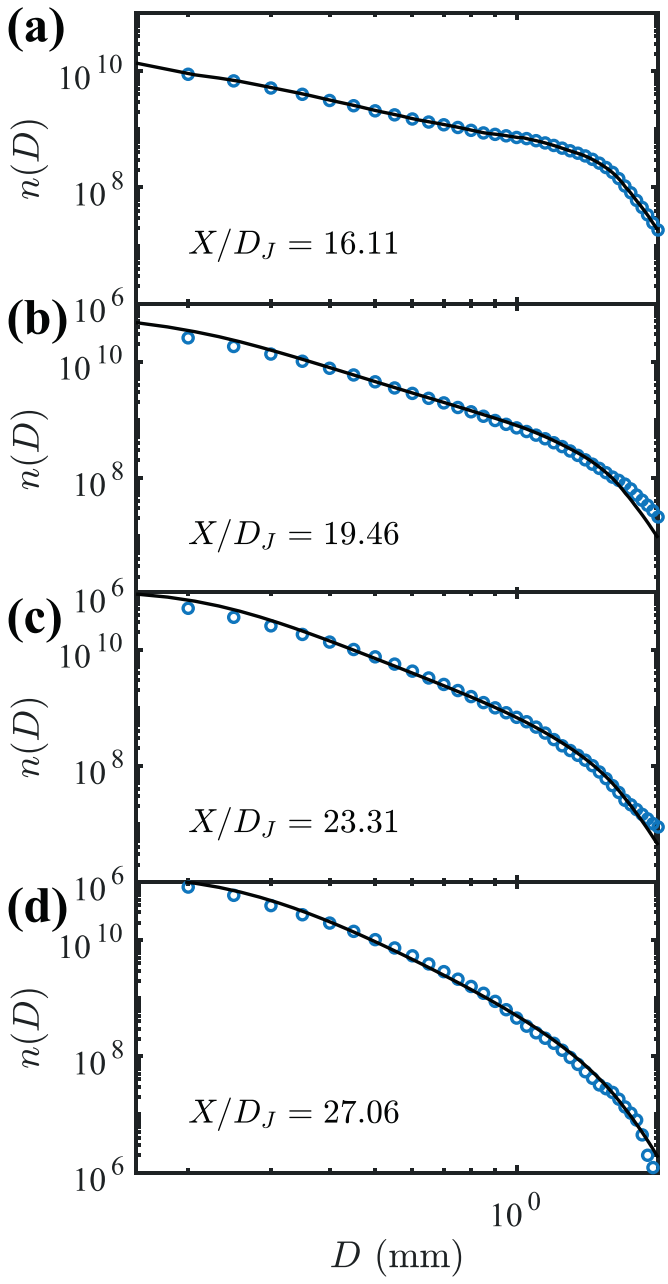

Fig. 11. Bubble size spectrum as a function of the distance between the measurement window to the nozzle exit X normalized by the nozzle diameter D_j. Blue circles denote the experimental results by Martínez-Bazán et al. (1999b). The black solid line show the simulation results obtained by implementing the new model using Eq. 7 for daughter bubble size distribution and Eq. (9) for breakup frequency. Data at $X/D_j = 16.11$ was used as the initial condition, so the symbols and the line in (a) are identical.

which may seem appealing because of their linkages with the underlying physics. But the possible involvements of so many mechanisms at play make it impossible to conclusively argue which physics dominates. Instead of following the same process, in this work, the simple form of our new model is completely born from experimental constraints. Moreover, since different aspects of daughter bubble size distribution could be magnified under different statistical lens, providing experimental data on other statistics in addition to the bubble spectrum in the future could potentially provide new constraints to the problem.

5. Conclusion

The population balance equation has served as an important tool to model bubble breakup and coalescence for gas-liquid two-phase flows. For breakup, daughter bubble size distribution is an unknown parameter that cannot be acquired from the first principle. As a result, there have been many attempts to model this distribution from physical phenomenological arguments, such as eddy-bubble collision. However, there seems to be no consensus as to what the basic trend of daughter bubble size distribution should be—it could be Bell-shape, U-shape, or M-shape.

In this paper, the goal is to find a model that satisfies the constraints put forward by consistent experimental results, including our own work and many others from the literature. In this paper, we first introduced our experimental setup with special attention paid to designing a system that can provide a large area of homogeneous and isotropic turbulent flows to study bubble breakup. This system also features a 3D shape reconstruction system consisting of six cameras to capture the breakup process and to accurately identify bubble sizes. Unlike the inconsistent models, the measured daughter size distribution agrees well with other previous experimental measurements (Hesketh et al., 1991; Rodríguez-Rodríguez et al., 2003; Vejražka et al., 2018).

Other than the direct measurement, the bubble size spectrum obtained by experiments (Deane and Stokes, 2002; Rojas and Loewen, 2007; Blenkinsopp and Chaplin, 2010; Martínez-Bazán et al., 1999a) offer other constraints on breakup models, including: (i) the -10/3 scaling law observed for bubbles larger than the Hinze scale; this scaling law seems to depend only on breakup frequency rather than daughter bubble size distribution; (ii) the negative sub-Hinze-scale bubble scaling (exponent close to -3/2) provides another constraint on the trend of daughter bubble size distribution for uneven breakup ($V^* \rightarrow 0$); (iii) the time evolution of bubble size spectrum, including the converged time in *continuous injection* cases (Fig. 7) and a continuous change in *one-time-injection* experiments (Fig. 11). Moreover, the breakup frequency model by Martínez-Bazán et al. (1999a) is corrected by incorporating the distribution of the turbulent energy dissipation rate.

The proposed framework provides a new way to develop bubble breakup model. Rather than starting from physical arguments, the new framework emphasizes on various experimental constraints and different reported statistics, which magnify different aspects of breakup models. A new model for daughter bubble size distribution is finally proposed and implemented in the population balance equation. Despite its simple formulation, the new model satisfies all experimental constraints that have been put forward.

Declaration of Competing Interest

The authors declare that they have no known competing financial interests or personal relationships that could have appeared to influence the work reported in this paper.

Supplementary material

Supplementary material associated with this article can be found, in the online version, at 10.1016/j.ijmultiphaseflow.2020.103397

CRediT authorship contribution statement

Yinghe Qi: Conceptualization, Formal analysis, Writing - original draft. **Ashik Ullah Mohammad Masuk:** Data curation. **Rui Ni:** Conceptualization, Supervision, Writing - review & editing.

References

Batchelor, G., 1956. The Theory of Homogeneous Turbulence. Cambridge Unviersity Press.

Blenkinsopp, C.E., Chaplin, J.R., 2010. Bubble size measurements in breaking waves using optical fiber phase detection probes. IEEE J. Oceanic Eng. 35 (2), 388–401.

Chan, W., Dodd, M.S., Johnson, P.L., Urzay, J., Moin, P., 2018. Formation and dynamics of bubbles in breaking waves: part II. the evolution of the bubble size distribution and breakup/coalescence statistics. Ann. Res. Briefs 21–34.

Coulaloglou, C.A., Tavlarides, L.L., 1977. Description of interaction processes in agitated liquid-liquid dispersions. Chem. Eng. Sci. 32 (11), 1289–1297.

Deane, G.B., Stokes, M.D., 2002. Scale dependence of bubble creation mechanisms in breaking waves. Nature 418 (6900), 839.

Deike, L., Melville, W.K., Popinet, S., 2016. Air entrainment and bubble statistics in breaking waves. J. Fluid Mech. 801, 91–129.

Garrett, C., Li, M., Farmer, D., 2000. The connection between bubble size spectra and energy dissipation rates in the upper ocean. J. Phys. Oceanogr. 30 (9), 2163–2171.

Hagesaether, L., Jakobsen, H.A., Svendsen, H.F., 2002. A model for turbulent binary breakup of dispersed fluid particles. Chem. Eng. Sci. 57 (16), 3251–3267.

Han, L., Luo, H., Liu, Y., 2011. A theoretical model for droplet breakup in turbulent dispersions. Chem. Eng. Sci. 66 (4), 766–776.

Hesketh, R.P., 1987. Bubble breakage in turbulent liquid flow. University of Delaware Ph.D. thesis.

Hesketh, R.P., Etchells, A.W., Russell, T.W.F., 1991. Experimental observations of bubble breakage in turbulent flow. Ind. Eng. Chem. Res. 30 (5), 835–841.

Hinze, J.O., 1955. Fundamentals of the hydrodynamic mechanism of splitting in dispersion processes. AIChE J. 1 (3), 289–295.

Hsia, M.A., Tavlarides, L.L., 1983. Simulation analysis of drop breakage, coalescence and micromixing in liquid-liquid stirred tanks. Chem. Eng. J. 26 (3), 189–199.

Kocamustafaogullari, G., Ishii, M., 1995. Foundation of the interfacial area transport equation and its closure relations. Int. J. Heat Mass Transf. 38 (3), 481–493.

Kolmogorov, A.N., 1941. The local structure of turbulence in incompressible viscous fluid for very large Reynolds numbers. Cr Acad. Sci. URSS 30, 301–305.

Kolmogorov, A.N., 1962. A refinement of previous hypotheses concerning the local structure of turbulence in a viscous incompressible fluid at high Reynolds number. J. Fluid Mech. 13 (1), 82–85.

Kutulakos, K.N., Seitz, S.M., 2000. A theory of shape by space carving. Int. J. Comput. Vis. 38 (3), 199–218.

Lamb, H., 1932. Hydrodynamics. Cambridge University Press.

Laurentini, A., 1994. The visual hull concept for silhouette-based image understanding. IEEE Trans. Pattern Anal. Mach. Intell. 16 (2), 150–162.

Lee, C.-H., Erickson, L.E., Glasgow, L.A., 1987. Bubble breakup and coalescence in turbulent gas-liquid dispersions. Chem. Eng. Commun. 59 (1–6), 65–84.

Lehr, F., Millies, M., Mewes, D., 2002. Bubble-size distributions and flow fields in bubble columns. AIChE J. 48 (11), 2426–2443.

Liao, Y., Lucas, D., 2009. A literature review of theoretical models for drop and bubble breakup in turbulent dispersions. Chem. Eng. Sci. 64 (15), 3389–3406.

Luo, H., Svendsen, H.F., 1996. Theoretical model for drop and bubble breakup in turbulent dispersions. AIChE J. 42 (5), 1225–1233.

Martínez-Bazán, C., 1998. Splitting and dispersion of bubbles by turbulence. University of California, San Diego.

Martínez-Bazán, C., Montanes, J.L., Lasheras, J.C., 1999a. On the breakup of an air bubble injected into a fully developed turbulent flow. part 1. breakup frequency. J. Fluid Mech. 401, 157–182.

Martínez-Bazán, C., Montanes, J.L., Lasheras, J.C., 1999b. On the breakup of an air bubble injected into a fully developed turbulent flow. part 2. size PDF of the resulting daughter bubbles. J. Fluid Mech. 401, 183–207.

Martínez-Bazán, C., RODRÍGUEZ-RODRÍGUEZ, J., Deane, G.B., Montanes, J.L., Lasheras, J.C., 2010. Considerations on bubble fragmentation models. J. Fluid Mech. 661, 159–177.

Masuk, A.U.M., Salibindla, A., Ni, R., 2019a. A robust virtual-camera 3d shape reconstruction of deforming bubbles/droplets with additional physical constraints. Int. J. Multiphase Flow 103088.

Masuk, A.U.M., Salibindla, A., Tan, S., Ni, R., 2019b. V-ONSET (Vertical octagonal noncorrosive stirred energetic turbulence): a vertical water tunnel with a large energy dissipation rate to study bubble/droplet deformation and breakup in strong turbulence. Rev. Sci. Instrum. 90 (8), 085105.

Matusik, W., Buehler, C., Raskar, R., Gortler, S.J., McMillan, L., 2000. Image-based visual hulls. In: Proceedings of the 27th Annual Conference on Computer Graphics and Interactive Techniques, pp. 369–374.

Meneveau, C., Sreenivasan, K.R., 1991. The multifractal nature of turbulent energy dissipation. J. Fluid Mech. 224, 429–484.

Mulayim, A.Y., Yilmaz, U., Atalay, V., 2003. Silhouette-based 3-d model reconstruction from multiple images. IEEE Trans. Syst. Man Cybern. Part B (Cybern.) 33 (4), 582–591.

Narsimhan, G., Gupta, J.P., Ramkrishna, D., 1979. A model for transitional breakage probability of droplets in agitated lean liquid-liquid dispersions. Chem. Eng. Sci. 34 (2), 257–265.

Ni, R., Xia, K.-Q., et al., 2013. Kolmogorov constants for the second-order structure function and the energy spectrum. Phys. Rev. E 87 (2), 023002.

Prince, M.J., Blanch, H.W., 1990. Bubble coalescence and break-up in air-sparged bubble columns. AIChE J. 36 (10), 1485–1499.

Rodríguez-Rodríguez, J., Martínez-Bazán, C., Montañés, J.L., 2003. A novel particle tracking and break-up detection algorithm: application to the turbulent break-up of bubbles. Meas. Sci. Technol. 14 (8), 1328.

Rojas, G., Loewen, M.R., 2007. Fiber-optic probe measurements of void fraction and bubble size distributions beneath breaking waves. Exp. Fluids 43 (6), 895–906.
Sreenivasan, K.R., 1995. On the universality of the Kolmogorov constant. Phys. Fluids 7 (11), 2778–2784.
Tsouris, C., Tavlarides, L.L., 1994. Breakage and coalescence models for drops in turbulent dispersions. AlChE J. 40 (3), 395–406.
Valentas, K.J., Bilous, O., Amundson, N.R., 1966. Analysis of breakage in dispersed phase systems. Ind. Eng. Chem. Fundam. 5 (2), 271–279.
Variano, E.A., Bodenschatz, E., Cowen, E.A., 2004. A random synthetic jet array driven turbulence tank. Exp. Fluids 37 (4), 613–615.
Vejražka, J., Zedníková, M., Stanovský, P., 2018. Experiments on breakup of bubbles in a turbulent flow. AlChE J. 64 (2), 740–757.
Wang, T., Wang, J., Jin, Y., 2003. A novel theoretical breakup kernel function for bubbles/droplets in a turbulent flow. Chem. Eng. Sci. 58 (20), 4629–4637.
Wang, Z., Yang, J., Stern, F., 2016. High-fidelity simulations of bubble, droplet and spray formation in breaking waves. J. Fluid Mech. 792, 307–327.
Williams, F.A., 1985. Combustion Theory. Addison-Wesley.
Yu, X., Hendrickson, K., Yue, D.K.P., 2020. Scale separation and dependence of entrainment bubble-size distribution in free-surface turbulence. J. Fluid Mech. 885.
Zhao, H., Ge, W., 2007. A theoretical bubble breakup model for slurry beds or three--phase fluidized beds under high pressure. Chem. Eng. Sci. 62 (1–2), 109–115.